6th European Conference on Computational Mechanics (ECCM 6)
7th European Conference on Computational Fluid Dynamics (ECFD 7)
1115 June 2018, Glasgow, UK

A-PRIORI STUDY OF WALL MODELING IN LARGE EDDY SIMULATION

S. REZAEIRAVESH[1], T. MUKHA[1], M. LIEFVENDAHL[1,2]

[1] Division of Scientific Computing, Uppsala University
Box 337, SE-751 05 Uppsala, Sweden
saleh.rezaeiravesh@it.uu.se, timofey.mukha@it.uu.se

[2] FOI, Totalförsvarets forskningsinstitut
SE-164 90 Stockholm, Sweden
mattias.liefvendahl@foi.se

Key words: Large eddy simulation, Wall modeling, Algebraic wall models

Abstract. The velocity signal of a high quality wall-resolving large eddy simulation (WRLES) of fully-developed turbulent channel flow at $\mathrm{Re}_\tau = 1000$ is spatially averaged over cubic boxes of size corresponding to possible choices for grid-cell size in a wall-modeled (WM)LES of the same flow. Two box sizes are considered, as well as multiple wall-normal locations of the center of the box. After applying filtering in time, the generated velocity signals are used to study algebraic wall models with respect to their ability to accurately predict the wall shear stress, $\bar{\tau}_w$. In particular, models based on the Spalding and Reichardt laws are examined. The sensitivity of $\bar{\tau}_w$ with respect to the wall-normal distance of the velocity sampling point, h, the wall model and its parameters, and also to the resolution of the WMLES grid is addressed. It is shown that by using wall models with the parameters calibrated to fit the WRLES mean velocity profiles, the mean of the wall shear stress can be accurately predicted, however, no improvement for the fluctuations of this quantity is achieved. To avoid dependence of the mean predicted $\bar{\tau}_w$ on h, an integrated formulation of algebraic wall models is proposed and applied to Reichardt law, leading to improved results. Finally, an idea is described and examined to increase the correlation between the predicted $\bar{\tau}_w$ and reference wall shear stress through dynamically adjusting the wall model parameters. To facilitate similar studies, the generated datasets for a-priori study of WMLES are made publicly available.

1 INTRODUCTION

The essential requirement for wall-resolving large eddy simulation (WRLES) is to resolve structures of the order of the local viscous length scale δ_ν, where $\delta_\nu = \nu/u_\tau$, in the turbulent boundary layer (TBL). Here, ν is the fluid kinematic viscosity and u_τ denotes the wall friction velocity defined as $u_\tau = \sqrt{\tau_w/\rho}$, with τ_w and ρ being magnitude of the wall shear stress and fluid density, respectively. This requirement results in excessive

growth of the number of grid cells with Reynolds (Re-)number, [5, 6, 18], which is the main barrier to applying WRLES to many real-life applications, [21]. In contrast, the requirement in the wall-modeled (WM)LES approach is to only directly resolve the flow structures in the outer part of the TBL, which scale with $\delta \gg \delta_\nu$. Consequently, the required number of grid cells is reduced, see [5, 6, 20], but the near-wall region in WM-LES is under-resolved and hence some appropriate type of wall modeling is required to approximate the uncaptured effects.

There have been various suggestions for wall modeling, see the reviews [15, 14, 10] and the references therein. In one approach, referred to as wall-stress modeling, a part of the near-wall modeling is devoted to predicting the correct value of the local wall shear stress, given information from the outer part of the TBL which is supposed to be sufficiently resolved. The focus of the present study is on so-called algebraic wall-stress models using laws of the wall valid for equilibrium TBLs, [16, 8], to make the predictions.

In what is hereafter called a-posteriori WMLES, at each time step, there is a coupling between the LES solution in the interior computational domain and the wall model which takes in information from the interior domain and then predicts and imposes a boundary condition for the LES equations at the wall. In the present study, similar to [3, 4, 7], the coupling between the flow solver and wall model at the wall is removed leading to a framework for a-priori WMLES within which the possibility of studying the performance of the wall model in predicting wall shear stress is provided.

The particular wall models used in the present study are shortly reviewed in Section 2. To generate velocity samples suitable for the wall model, the velocity field of a high-quality WRLES of channel flow at $\mathrm{Re}_\tau = u_\tau \delta/\nu = 1000$, where δ denotes the channel half-height, is filtered in both space and time. The details of the procedure are found in Section 3. Moreover, the reference wall shear stress to which the wall models' predictions are compared is introduced. As a main objective of the present study, the sensitivity of the predicted wall shear stress with respect to different factors is investigated in Section 4.1. In order to remove the observed dependency of the predictions on the sampling height, an integrated formulation of algebraic wall models is proposed. In the end, in Section 4.3, the possibility of using an algebraic wall model with dynamically-adjustable parameters to enhance capability of predicting fluctuations of wall shear stress is discussed.

2 ALGEBRAIC WALL MODELS

The inner-scaled laws of the wall developed for equilibrium TBLs can be used as algebraic wall models. In their general form, these laws read as, $F\left(q, y^+, \langle u\rangle^+\right) = 0$, where, q are the model parameters and taken to be fixed, $\langle\cdot\rangle$ denotes the mean value, $\langle u\rangle^+ = \langle u\rangle/\langle u_\tau\rangle$ and $y^+ = y\langle u_\tau\rangle/\nu$ represent the inner-scaled mean velocity and distance from the wall, respectively. At any specific point on the wall with coordinates (x, z), the local mean friction velocity $\langle u_\tau\rangle$ is defined as $\sqrt{\langle\tau_w\rangle/\rho}$. In WMLES, it is assumed that the law of the wall also holds for the instantaneous filtered velocity $\bar{u}$ sampled at distance y from the wall. As a result, the associated local instantaneous $\bar{u}_\tau(x, z, y, t)$ is iteratively predicted from,

$$F(\bar{u}_\tau, q, y, \bar{u}) = 0\,. \tag{1}$$

The two particular wall models considered in Section 4 cover the distance between the wall up to the wake region (i.e. the end of outer layer) of the TBL, see e.g. [16]. The first model is proposed by Spalding, [23],

$$y^+ = \langle u \rangle^+ + e^{-\kappa B}\left[e^{\kappa\langle u\rangle^+} - \sum_{m=0}^{3}\frac{(\kappa\langle u\rangle^+)^m}{m!}\right], \tag{2}$$

with default parameters $\kappa = 0.4$ and $B = 5.5$. The second one is that of Reichardt [17],

$$\langle u \rangle^+ = \frac{1}{\kappa}\ln\left(1+\kappa y^+\right) + C\left[1 - e^{-\frac{y^+}{B_1}} - \frac{y^+}{B_1}e^{-\frac{y^+}{B_2}}\right], \tag{3}$$

with default parameters $\kappa = 0.4$, $C = 7.8$, $B_1 = 11$, and $B_2 = 3$.

3 DATA FOR a-PRIORI WMLES

In order to generate the velocity samples used by the wall model, high quality data of WRLES of fully-developed turbulent channel flow at nominal $\mathrm{Re}_\tau = 1000$ are utilized. The details of the WRLES are summarized in Table 1. Also, the resulting profiles of a number of velocity statistical moments, which agree very well with the reference DNS data of [11], are shown in Fig. 1. To perform this simulation, the open-source finite-volume based library OpenFOAM, see [12] and the references therein, was employed. Nominally second-order accurate schemes for discretization in both space and time are used with constant time step size $\Delta t_R = 0.002$. Moreover, no explicit subgrid-scale (SGS) modeling was included in the simulation. For further details, see [19].

Table 1: Details of WRLES of channel flow at target $\mathrm{Re}_\tau = 1000$. The physical parameters are bulk velocity $U_b = 1$ m/s, channel half-height $\delta = 1$ m and $\nu = 5\times10^{-5}$ m^2/s, which result in $\mathrm{Re}_\tau = 1000.512$ according to DNS, [11]. The inner-scaled wall-normal distance of the first off-wall cell center and the cell size in wall-normal direction at the center of the channel are denoted by Δy_w^+ and Δy_c^+, respectively.

Re_τ	Resolution				Domain Size	No. of Cells
	Δx^+	Δz^+	Δy_w^+	Δy_c^+	$l_x \times l_y \times l_z$	
986	16.6	10	0.445	40	$9\delta \times 2\delta \times 4\delta$	$543 \times 116 \times 403$

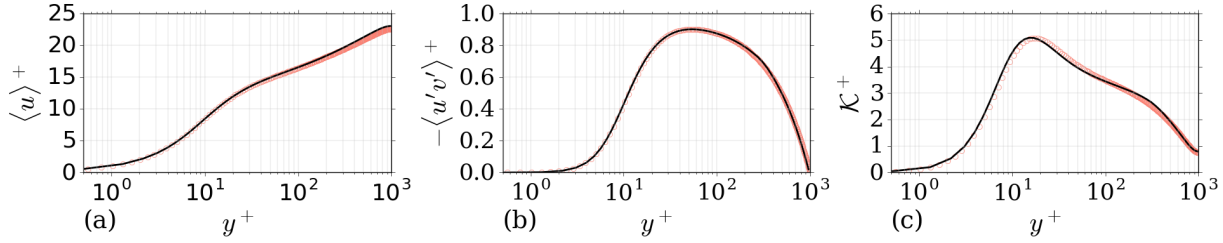

Figure 1: Inner-scaled profile of WRLES mean velocity (a), Reynolds stress (b) and turbulent kinetic energy (c) compared to the DNS data of [11] (symbols).

The velocity field of the WRLES is, in the course of simulation, spatially averaged over the volume of cubic boxes centered around the points with coordinates $\mathbf{x}_M = (x_M, h, z_M)$, where x_M and z_M are fixed (associated to a point on the wall) and h specifies different heights from the wall. Due to periodicity, the choice of x_M and z_M is arbitrary, and is here chosen to be the centroid of the wall. By filtering in time, in the post-processing stage, the WMLES velocity signals are generated via,

$$\bar{\mathbf{u}}(\mathbf{x}_M, t) = \frac{1}{\Delta t_M V_M} \int_{\Delta t_M} \int_{V_M} \mathbf{u}(\mathbf{x} - \mathbf{x}_M, t^*) \mathrm{d}\mathbf{x}\, \mathrm{d}t^* \,, \tag{4}$$

where, boldface letters represent vectors, $\Delta t_M = N_t \Delta t_R$ with $N_t > 1$ specifies time step size associated with WMLES, and $V_M = (\delta/n)^3$ is the volume of the cubic boxes which mimic the WMLES cells. In the present study, two different resolutions $n = 20$ and 30 are considered. A total of n sampling points $\mathbf{x}_{M_i} = (x_M, h_i, z_M)$, where $i = 1, 2, \cdots, n$, is chosen so that they cover the distance between the wall and the channel half-height δ, i.e. $h_i = (2i-1)\delta/(2n)$. A velocity snapshot of the WRLES with the associated grid along with the schematic representation of the WMLES cells are illustrated in Fig. 2.

In total, 213 000 time-samples of WRLES velocity $\mathbf{u}$, corresponding to more than 47 flow-through times are uniformly filtered (i.e. averaged with the same weights) to generate WMLES velocity signals $\bar{\mathbf{u}}$. In particular, $N_t = \Delta t_M / \Delta t_R$ is chosen to be 10, in accordance with the time step size practically used for a-posteriori WMLES.

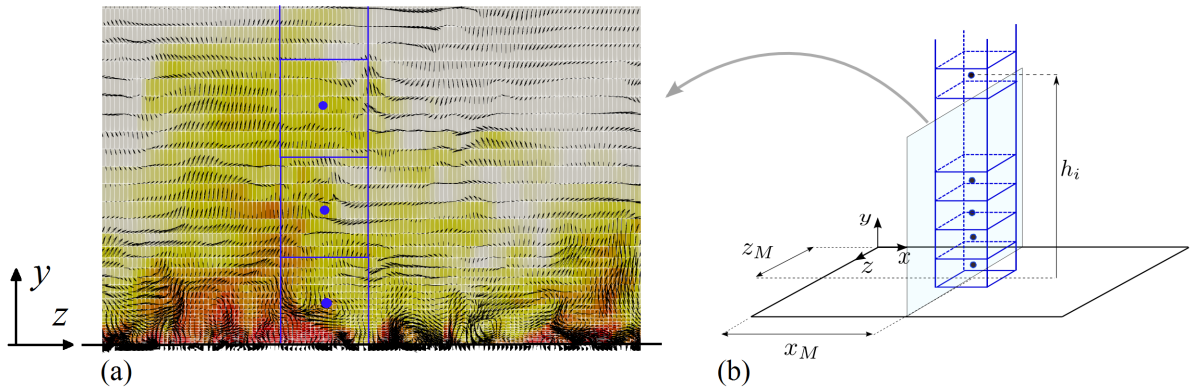

Figure 2: Instantaneous velocity field of the WRLES of channel flow at $\mathrm{Re}_\tau = 1000$ (a), with cells represented by gray lines. The blue boxes (a,b) schematically show the WMLES cells with volume $(\delta/n)^3$ over which the WRLES fields are averaged.

In addition to the WMLES cells for sampling velocity in the interior of the domain, another box with volume $\delta/n \times 2\Delta y_w \times \delta/n$ is considered adjacent to the wall with center at $(x_M, \Delta y_w, z_M)$. Since this center is located in the viscous sublayer of the TBL, a reference wall shear stress associated to the volume can be directly calculated as $\tau_{w_M} = \rho\nu\bar{u}_M/\Delta y_w$. The velocity samples $\bar{u}_M$ are calculated in the same way as in (4) but employing the volume $\delta/n \times 2\Delta y_w \times \delta/n$ instead. For comparison, the wall shear stress signal from WRLES, τ_{w_R}, is also computed using the WRLES velocity at $(x_M, \Delta y_w, z_M)$ filtered in time.

Table 2: Comparison between reference wall shear stresses.

Wall shear stress	n	$\langle\tau_w\rangle \times 10^3$	$\tau_w'^+$	Correlation with τ_{w_R}
τ_{w_R}	-	2.560	0.418	1.000
τ_{w_M}	20	2.573	0.288	0.794
τ_{w_M}	30	2.579	0.330	0.878

According to the quantitative comparison in Table 2, only τ_{w_R} has physically correct value of normalized fluctuations $\tau_w'^+ = \text{sdev}(\tau_w)/\langle\tau_w\rangle$ which is known to be ≈ 0.4 [1] with small increase with Re-number, see [13]. Here, sdev$(\cdot)$ represents standard deviation. When WMLES resolution n increases, both $\tau_w'^+$ and the correlation between τ_{w_M} and τ_{w_R} grow. The latter is clearly observable from the scatter plots in Fig. 3. Also shown in this figure are the marginal probability density functions (PDF) of $\tau^+_{w_M} = \tau_{w_M}/\langle\tau_{w_M}\rangle$ and $\tau^+_{w_R} = \tau_{w_R}/\langle\tau_{w_R}\rangle$. According to Alfredsson et al. [2], $\tau^+_{w_R}$ signals have log-normal distribution. The same type of distribution can be also fitted to $\tau^+_{w_M}$, although with slightly different parameters than those for $\tau^+_{w_R}$.

In order to evaluate the performance of the wall models in Section 4, a reference wall shear stress is required which is chosen to be τ_{w_M}. Taking into account the deviation of τ_{w_M} from the "true" wall shear stress τ_{w_R}, it is accepted that even a perfect wall model is not supposed to predict the physically true values of wall shear stress.

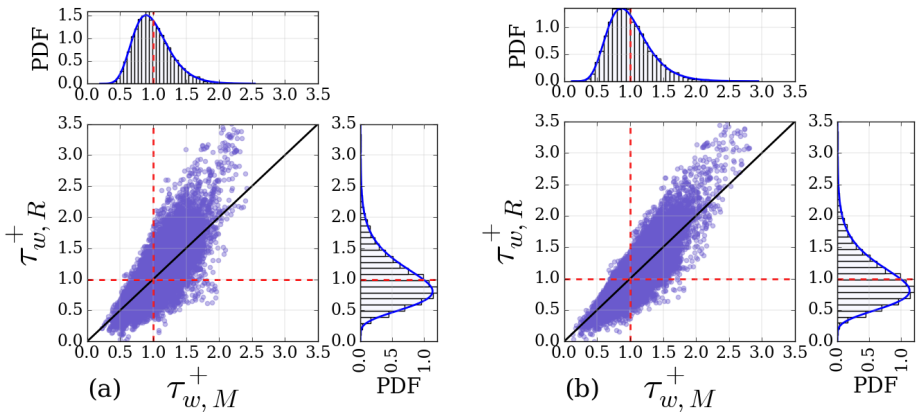

Figure 3: Scatter plot and marginal PDF of $\tau^+_{w_M}$ and $\tau^+_{w_R}$ for $n = 20$ (a) and $n = 30$ (b). The solid blue lines represent the log-normal PDFs fitted to the samples. The red dashed lines represent mean values.

4 PERFORMANCE OF ALGEBRAIC WALL MODELS

4.1 Factors influencing the predictions of wall models

Different factors can potentially influence the predictions of the wall shear stress in wall modeling. In particular, the algebraic wall model and its parameter values, the wall-normal distance to the velocity sampling point, h, the characteristics of the sampled streamwise velocity component imported to the wall model, $\bar{u}$, and grid resolution n are the potentially most influential factors. Here, an attempt is made to assess the influence

of these factors using the WMLES data of Section 3.

The normalized error in $\langle \bar{u}_\tau \rangle$, predicted by two wall models and different parameter values at different h/δ is shown in Fig. 4(a). This error is defined as, $\epsilon[\langle \bar{u}_\tau \rangle] = (\langle \bar{u}_\tau \rangle - \langle u_{\tau_M} \rangle)/\langle u_{\tau_M} \rangle$ where $u_{\tau_M} = \sqrt{\tau_{w_M}/\rho}$. Independent of the wall model and parameters used, sampling from the closest WMLES cell center to the wall results in the largest magnitude of $\epsilon[\langle \bar{u}_\tau \rangle]$. This is in agreement with what is observed in a-posteriori WMLES, see e.g. [9]. By increasing h/δ, the value of $\epsilon[\langle \bar{u}_\tau \rangle]$ changes, however, it becomes almost fixed for $h/\delta \gtrsim 0.6$ associated with the wake region of the TBL. The latter is due to the fact that both Spalding and Reichardt wall models are valid up to the end of the outer layer. A more interesting observation is that below the wake region, the choice of parameter values can vertically shift the $\epsilon[\langle \bar{u}_\tau \rangle]$-$h/\delta$ graph. When both the Spalding and Reichardt laws are used with the parameters calibrated to fit the $\langle u \rangle^+$-y^+ profile of the WRLES, similar negligible $\epsilon[\langle \bar{u}_\tau \rangle]$ is observed for sampling velocity from the overlap region of the TBL, see the red and yellow graphs in Fig. 4(a).

To quantify how sensitive the predicted $\bar{u}_\tau$ are to the variations of the wall model parameters and sampling velocity $\bar{u}$, local sensitivity analysis, see e.g. [22], is performed for the wall models (2) and (3). The resulting expression in its general form is written as,

$$\frac{\Delta \bar{u}_\tau}{\bar{u}_{\tau_0}} = \chi_{\bar{u}} \frac{\Delta \bar{u}}{\bar{u}_0} + \sum_{i=1} \chi_{q_i} \frac{\Delta q_i}{q_{0_i}}, \tag{5}$$

where subscript 0 shows the nominal value of a quantity, Δ denotes small deviation from the nominal values, and χ represent the local sensitivity indices. In particular, the nominal wall model parameters are chosen to be corresponding default values (see Section 2), $\bar{u}_0$ is taken to be $\langle \bar{u} \rangle$, and $\bar{u}_{\tau_0}$ is the prediction of the wall model for $\bar{u}_0$ and q_0. According to Fig. 4(b) and (c), $\bar{u}_\tau$ is most sensitive to $\bar{u}$ and then to a lower extent to the wall model parameters. $\chi_{\bar{u}}$ is almost unchanged with h/δ, however, since $\mathrm{sdev}(\bar{u})/\langle \bar{u} \rangle$ decreases with h/δ, the overall impact of $\bar{u}$ on $\Delta \bar{u}_\tau / \bar{u}_{\tau_0}$ reduces at higher h/δ. Note that, similar results were obtained for $n = 30$.

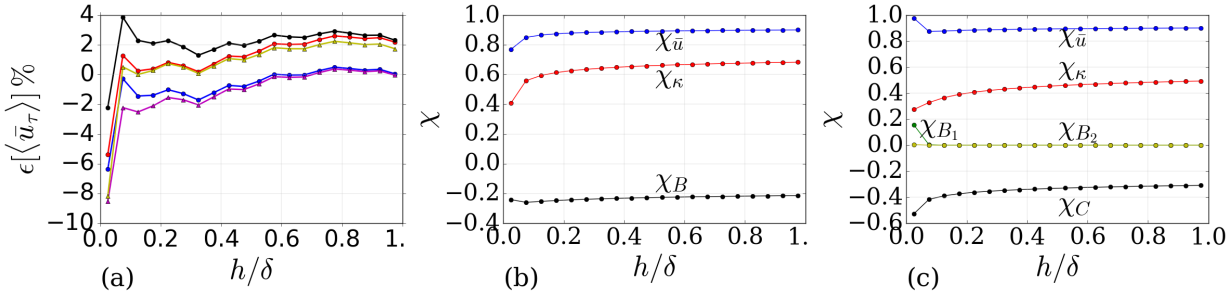

Figure 4: Variation of the normalized error in predicted $\langle \bar{u}_\tau \rangle$ with h/δ for $n = 20$ (a) when the Spalding law with κ, B = 0.4, 5.5 (blue), 0.415, 5.6 (red), 0.38, 4.0 (black), and the Reichardt law with κ, C, B_1, B_2 = 0.4, 7.8, 11, 3.0 (magenta) and 0.395, 7.2, 8.0, 4.0 (yellow) are used. The local sensitivity indices for the $\bar{u}_\tau$ predicted by the Spalding law (b), and the Reichardt law (c) for default parameter values and $n = 20$.

It is also interesting to evaluate the ability of the wall models to predict the fluctuations in $\bar{u}_\tau$. For the same set of wall models and their parameters as above, Fig. 5 illustrates the error in the normalized fluctuations of the wall friction velocity, i.e. $\bar{u}_\tau'^{+} = \mathrm{sdev}(\bar{u}_\tau)/\langle\bar{u}_\tau\rangle$, and also the correlation coefficient between $\bar{u}_\tau$ predicted by a wall model and the reference u_{τ_M}. As h/δ increases, the magnitude of $\epsilon[\bar{u}_\tau'^{+}]$ grows and $\mathrm{cor}(\bar{u}_\tau, u_{\tau_M})$ decreases. Neither changing the wall model and its parameters nor the WMLES resolution n make any difference in these trends. These observations are somewhat expected: at higher distances from the wall, $\mathrm{sdev}(\bar{u})/\langle\bar{u}\rangle$ reduces and $\bar{u}$ becomes less correlated with the wall friction velocity. The lack of dependency of $\epsilon[\bar{u}_\tau'^{+}]$ on q follows from the fact that q are kept fixed and consequently do not affect the fluctuations of $\bar{u}_\tau$.

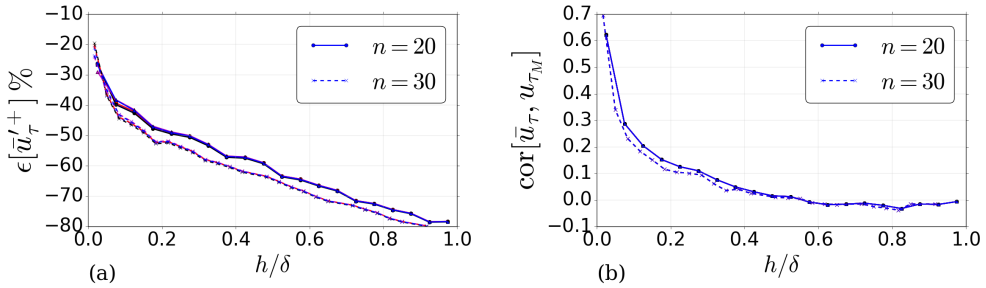

Figure 5: Variation of the normalized errors in $\bar{u}_\tau'^{+}$ (a), and the correlation between $\bar{u}_\tau$ and u_{τ_M} (b) with h/δ for parameters changing as in Fig. 4(a).

Combining the above observations, it is concluded that to accurately predict $\langle\bar{u}_\tau\rangle$, the use of a-priori tuned-up parameters q based on accurate benchmark $\langle u\rangle^+$-y^+ is necessary. However, as shown in Fig. 6, the optimized values of q vary with h/δ, although the variations become less significant as h/δ increases. When $\bar{u}$ is sampled from the wall-adjacent cell center, the magnitude of $\epsilon[\langle\bar{u}_\tau\rangle]$ for different combinations of κ and B is lower than when $\bar{u}$ is sampled from cells at higher h/δ. Also, the most accurate predictions of the fluctuations of $\bar{u}_\tau$ are obtained when the velocity samples are taken from the closest WMLES cell center to the wall. However, this may not be applicable to a-posteriori WMLES, where the flow may be under-resolved in the first few cells near the wall, see e.g. [9].

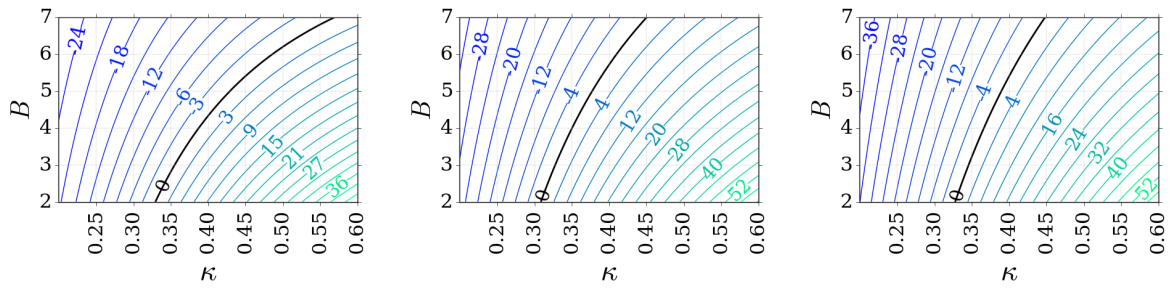

Figure 6: Isolines of $\epsilon[\langle\bar{u}_\tau\rangle]$ % for different combinations of parameters when Spalding law is used with $n = 20$. Input $\bar{u}$ to the wall model is sampled from (left to right) $h/\delta = 0.025, 0.075, 0.325$, associated to the first, second, and seventh cell centers of the WMLES grid. The black line shows $\epsilon[\langle\bar{u}_\tau\rangle] = 0$.

4.2 Integrated formulation of wall models

In Section 4.1 it was shown that in the standard use of wall models, while the error in $\langle \bar{u}_\tau \rangle$ can be minimized by the choice of the wall model parameters, q, the optimal values of q are dependent on h. Further, a significantly larger $\epsilon[\langle \bar{u}_\tau \rangle]$ was observed when h was set to the distance to the wall-adjacent WMLES cell center. Here, an approach for reducing the dependency of $\epsilon[\langle \bar{u}_\tau \rangle]$ on h is proposed. The idea is based on the the work of Werner and Wengle [24]. Note that, given some wall model which can be written as $\langle u \rangle^+ = F(\langle u_\tau \rangle, y, q)$, the wall-normal average of $\langle u \rangle$ over the interval $[h_1, h_2]$ can be expressed as,

$$\frac{1}{h_2 - h_1} \int_{h_1}^{h_2} \langle u \rangle \mathrm{d}y = \frac{\langle u_\tau \rangle}{h_2 - h_1} \int_{h_1}^{h_2} F(\langle u_\tau \rangle, y, q) \mathrm{d}y. \tag{6}$$

In the framework of collocated finite volume discretization, the values stored at the cell centers represent the volumetric averages of the unknowns across the corresponding cells. Therefore, it can be argued that in this setting, $\bar{u}$, taken from a cell center located at a wall-normal distance $0.5(h_1 + h_2)$, better approximates the left-hand-side of (6) rather than $\langle u \rangle$ itself. Adopting this hypothesis leads to the following equation for computing $\bar{u}_\tau$,

$$(h_2 - h_1)\bar{u} - \bar{u}_\tau \int_{h_1}^{h_2} F(\bar{u}_\tau, y, q) \mathrm{d}y = 0. \tag{7}$$

Two ways of applying (7) are considered here. One is to integrate over a single cell, with the cell center at a distance h from the wall. In this case, h_1 and h_2 are the lower and upper wall-normal bounds of the cell, respectively. The second way involves integrating over multiple consecutive off-the-wall cells. Then, h_1 is set to zero, h_2 is the upper bound of the upper-most cell, and the value of $\bar{u}$ is computed as the wall-normal average of the WMLES velocity across all the considered cells.

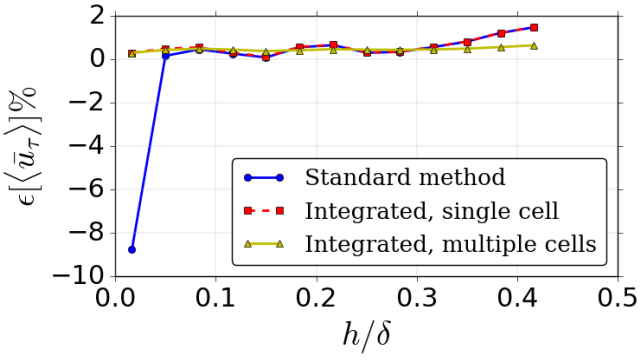

Figure 7: Error in the mean predicted friction velocity, $\langle \bar{u}_\tau \rangle$, as a function of the normalized distance to the sampling point, h/δ. In the case of integration across multiple cells, h refers to the cell center of the upper-most considered cell. Here, $n = 30$, and Reichardt law (3) with the following parameters is used $\kappa = 0.395$, $C = 7.2$, $B_1 = 8$, $B_2 = 4$.

Figure 7 shows the error in $\langle \bar{u}_\tau \rangle$ as function of h/δ, with Reichard law (3) used as F. It is observed that compared to the standard method, integrating over a single cell significantly

reduces the error, when $\bar{u}$ is taken from the wall-adjacent cell. Integrating over multiple cells stabilizes the behavior of the error across the whole considered range of h/δ.

4.3 Wall models with dynamically-adjusted parameters

As discussed in Section 4.1, algebraic wall models in their standard form, i.e. with constant parameters, can, at best, only accurately predict $\langle \bar{u}_\tau \rangle$. Here as a deviation from the standard form, the possibility of having non-fixed q in the course of wall modeling is investigated. Assume the reference wall friction velocity and signals of $\bar{u}$ at different h/δ are given and the parameters in wall model (1) are allowed to be adjusted for each joint sample of u_{τ_M} and $\bar{u}$. The aim is to see what the resulting joint PDF of the parameters would be. To this end, the following algorithm is considered. At each Δt_M, take $u_\tau^* = u_{\tau_M}$; then,

1. at $n_l \leq n$ heights from the wall associated with the cell centers of WMLES grid, find inner scaled velocity and wall-normal distance,

$$\bar{u}_i^* = \bar{u}_i / u_\tau^*, \quad y_i^* = h_i u_\tau^* / \nu, \quad \text{for} \quad i = 1, 2, \cdots, n_l \,.$$

2. Estimate κ^* and B^* from the logarithmic law of the wall using ordinary least square (OLS) method,

$$\kappa^{*^{-1}} = \frac{n_l \sum_{i=1}^{n_l} (\bar{u}_i^* \ln y_i^*) - (\sum_{i=1}^{n_l} \bar{u}_i^*)(\sum_{i=1}^{n_l} \ln y_i^*)}{n_l \sum_{i=1}^{n_l} (\ln y_i^*)^2 - (\sum_{i=1}^{n_l} \ln y_i^*)^2} \,, \quad B^* = \frac{1}{n_l} \sum_{i=1}^{n_l} \left[\bar{u}_i^* - \kappa^{*^{-1}} \ln y_i^* \right] \,.$$

3. Use, for instance, Spalding law (2) with κ^* and B^*, and $\bar{u}$ at any h to estimate $\bar{u}_\tau$.

By using the data of Section 3, joint samples of κ and B (conditioned on the u_{τ_M} and $\bar{u}$ data) shown in Fig. 8(a) are obtained. Although the marginal PDFs of B and κ seem to be respectively normal and non-normal, further studies employing Bayesian parameter estimation techniques is required to specify the PDF types more accurately. Here, the mean value of the parameters are found to be $\langle \kappa \rangle = 0.364$ and $\langle B \rangle = 2.645$, which are less than the standard values. However, these mean values are approximately on the zero-error loci in Fig. 6.

It should be noted that in the second step of the algorithm, logarithmic law is chosen because of its linear dependency on the parameters which makes applying the OLS method valid and accurate. In the third step, independent of h/δ, approximately the same mean and standard deviation of $\bar{u}_\tau$ and also the same correlation between $\bar{u}_\tau$ and u_{τ_M} are achieved. The latter is ≈ 0.91 and can be observed from Fig. 8(b-e).

To examine the idea of self-adjusted parameters in a-posteriori WMLES, the above algorithm should be iterative starting from an initial guess for u_τ^*. Once the difference between $\bar{u}_\tau$ estimated from step 3 and the starting u_τ^* is low, the iteration stops. Implementing such algorithm requires further study.

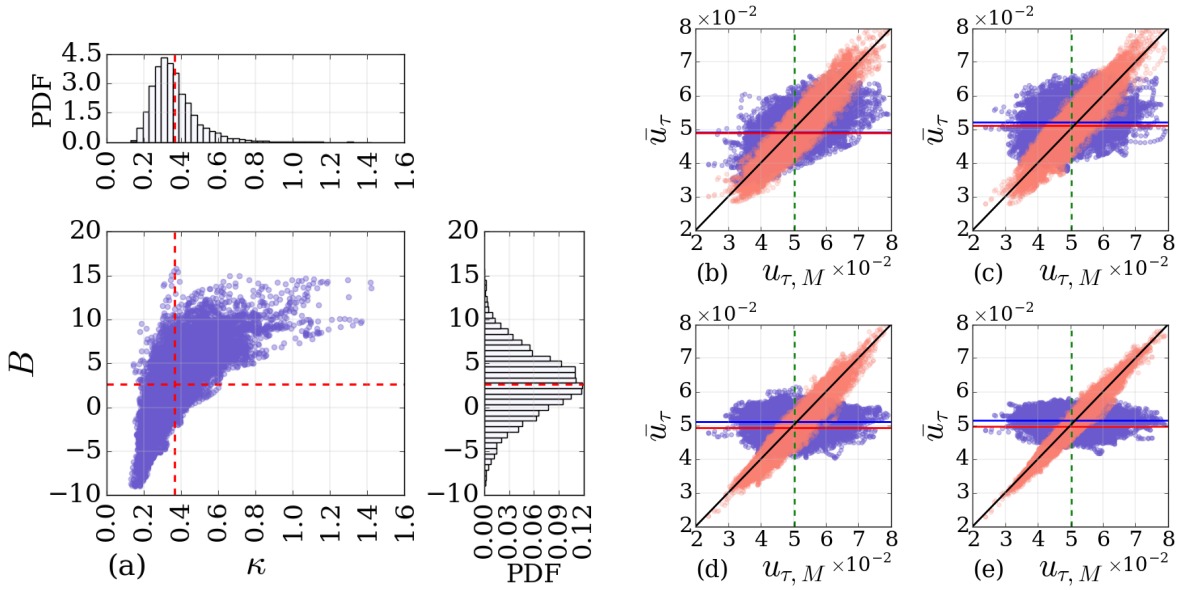

Figure 8: Scatter plot and PDFs of the dynamically adjusted κ and B (a). Scatter plots of $\bar{u}_\tau$ and u_{τ_M} (b-e) for $\bar{u}$ sampled from $h/\delta = 0.025$ (b), 0.075 (c), 0.375 (d), and 0.625 (e) in the WMLES with resolution $n = 20$. Dots and lines of the same color respectively show $\bar{u}_\tau$ and $\langle \bar{u}_\tau \rangle$ predicted by Spalding law with fixed (blue) and dynamically adjusted parameters (red). The green dashed line represents $\langle u_{\tau_M} \rangle$.

5 CONCLUSIONS

The performance of two algebraic wall models, the Spalding and Reichardt laws, equations (2) and (3), respectively, in predicting wall shear stress is studied in the framework of a-priori WMLES. To construct this framework, the input velocity samples to the wall models are generated by spatial and temporal filtering of the velocity field of a high-quality WRLES of channel flow at $\mathrm{Re}_\tau = 1000$, as detailed in Section 3.

In Section 4.1, the sensitivity of the wall models' predictions, $\bar{u}_\tau$, with respect to different factors is investigated. According to Fig. 4, the error in the mean value of the predicted friction velocity, $\langle \bar{u}_\tau \rangle$, varies with the wall-normal distance to the velocity sampling point, h/δ, the wall model used and its parameters q. Based on the local sensitivity analysis (5), the predicted $\bar{u}_\tau$ is most sensitive to the velocity samples $\bar{u}$ and then to the von Kármán parameter κ in the wall models. As shown in Fig. 6, depending on h/δ, there are different optimum values of the wall model parameters which result in accurate $\langle \bar{u}_\tau \rangle$. However, neither the wall model and different combinations of its parameters, nor the grid resolution improve the predicted fluctuations of $\bar{u}_\tau$, see Fig. 5. As demonstrated in Fig. 7, by using an integrated formulation of the wall model the dependency of $\langle \bar{u}_\tau \rangle$ on h/δ is removed and improved results are obtained. In Section 4.3, an algorithm is proposed and tested to increase the correlation between predicted $\bar{u}_\tau$ and the reference value through dynamically adjusting the wall model parameters. For this purpose, velocity samples in a column of WMLES cells with centers along the line perpendicular to the cell of interest on the wall are used. The described framework for a-priori WMLES can be seen as a complement to a-posteriori WMLES, which facilitates the evaluation of

different modifications and ideas. In this regard, the acquired datasets of velocity signals discussed in Section 3 are made publicly accessible [1].

ACKNOWLEDGEMENTS

The WRLES of channel flow was performed on resources provided by the Swedish National Infrastructure for Computing (SNIC) at PDC Centre for High Performance Computing (PDC-HPC). The study was supported by grant No 621-2012-3721 from the Swedish Research Council.

REFERENCES

[1] P. H. Alfredsson, A. V. Johansson, J. H. Haritonidis, and H. Eckelmann. The fluctuating wall-shear stress and the velocity field in the viscous sublayer. *The Physics of Fluids*, 31(5):1026–1033, 1988.

[2] P. H. Alfredsson, R. Örlü, and P. Schlatter. The viscous sublayer revisited-exploiting self-similarity to determine the wall position and friction velocity. *Experiments in Fluids*, 51(1):271–280, 2011.

[3] W. Cabot. Large-eddy simulations with wall models. *Center for Turbulence Research, Annual Research Brief*, pages 41–50, 1995.

[4] O. Cabrit, R. Mathis, V. Kulandaivelu, and I. Marusic. Towards a statistically accurate wall-model for large-eddy simulation. In *18th Australasian Fluid Mechanics Conference*, pages 2.1–2.5, 2012. Launceston, Australia.

[5] D. R. Chapman. Computational aerodynamics development and outlook. *AIAA journal*, 17(12):1293–1313, 1979.

[6] H. Choi and P. Moin. Grid-point requirements for large eddy simulation: Chapman's estimates revisited. *Physics of Fluids*, 24(1):–, 2012.

[7] J. Graham, K. Kanov, X. I. A. Yang, M. Lee, N. Malaya, C. C. Lalescu, R. Burns, G. Eyink, A. Szalay, R. D. Moser, and C. Meneveau. A web services accessible database of turbulent channel flow and its use for testing a new integral wall model for LES. *Journal of Turbulence*, 17(2):181–215, 2016.

[8] G. Grötzbach. *Direct numerical and large eddy simulation of turbulent channel flows. Encyclopedia of Fluid Mechanics, Ed. N. P. Cheremisinoff*, volume 6. 1987.

[9] S. Kawai and J. Larsson. Wall-modeling in large eddy simulation: Length scales, grid resolution, and accuracy. *Physics of Fluids*, 24(1):015105, 2012.

[10] J. Larsson, S. Kawai, J. Bodart, and I. Bermejo-Moreno. Large eddy simulation with modeled wall-stress: recent progress and future directions. *Bulletin of the JSME*, 3(1), 2016.

[1] DOI: 10.6084/m9.figshare.6052817.v1

[11] M. Lee and R. D. Moser. Direct numerical simulation of turbulent channel flow up to $Re_\tau \approx 5200$. *Journal of Fluid Mechanics*, 774:395415, 2015.

[12] T. Marić, J. Höpken, and K. Mooney. *The OpenFOAM Technology Primer*. sourceFlux, 2014.

[13] R. Örlü and P. Schlatter. On the fluctuating wall-shear stress in zero pressure-gradient turbulent boundary layer flows. *Physics of Fluids*, 23(2):021704, 2011.

[14] U. Piomelli. Wall-layer models for large-eddy simulations. *Progress in Aerospace Sciences*, 44(6):437 – 446, 2008.

[15] U. Piomelli and E. Balaras. Wall-layer models for large-eddy simulations. *Annu. Rev. Fluid Mech.*, 34:34974, 2002.

[16] S. B. Pope. *Turbulent Flows*. Cambridge University Press, 10th printing edition, 2000.

[17] V. H. Reichardt. Vollständige darstellung der turbulenten geschwindigkeitsverteilung in glatten leitungen. *Z. angew. Math. Mech.*, 31(7):208–219, 1951.

[18] S. Rezaeiravesh and M. Liefvendahl. Grid construction strategies for wall-resolving large eddy simulation and estimates of the resulting number of grid points. Technical Report 2017-005, Department of Information Technology, Uppsala University, 2017.

[19] S. Rezaeiravesh and M. Liefvendahl. Effect of grid resolution on large eddy simulation of wall-bounded turbulence. *arXiv:1804.01757v1 [physics.flu-dyn]*, 2018.

[20] S. Rezaeiravesh, M. Liefvendahl, and C. Fureby. On grid resolution requirements for LES of wall-bounded flows. In *Proceedings of the 7th ECCOMAS Congress*, volume 4, pages 7454–7465, 2016.

[21] J. Slotnick, A. Khodadoust, J. Alonso, D. Darmofal, W. Gropp, E. Laurie, and D. Marviplis. CFD vision 2030 study: A path to revolutionaty computational aerosciences. *NASA Technical Report*, 2014-218178, 2014.

[22] R. C. Smith. *Uncertainty Quantification Theory, Implementation, and Applications*. SIAM, 1st edition, 2014.

[23] D. B. Spalding. A single formula for the law of the wall. *ASME J. Appl. Mech.*, 28(3), 1961.

[24] H. Werner and H. Wengle. Large-eddy simulation of turbulent flow over and around a cube in a plate channel. In *Turbulent Shear Flows 8*, pages 155–168. Springer-Verlag, 1991.